ASIA-PACIFIC JOURNAL OF ATMOSPHERIC SCIENCES, 45, 4, 2009, p. 513-522

Investigation of Stratospheric Precursor for the East Asian Cold Surge Using the Potential Vorticity Inversion Technique

Baek-Min Kim[1], Jee-Hoon Jeong[2] and Seong-Joong Kim[1]

[1]*Korea Polar Research Institute, Inchon, Korea*
[2]*Department of Earth Sciences, University of Gothenburg, Gothenburg 405 30, Sweden*
(Manuscript received 18 September 2009; in final form 11 November 2009)

Abstract

The downward influence of stratospheric potential vorticity (PV) on the cold surge occurrence over East Asia was examined. Strong negative PV anomalies in the upper stratosphere and the rising of geopotential height in the upper troposphere about one week ahead of the cold surge occurrence were suggested as precursory perturbations triggering the development of the cold surge, which is dynamically validated by the piecewise potential vorticity inversion technique. When the inversion is applied to the stratospheric PV anomalies, geopotential and temperature anomalies balanced to the stratospheric PV were remarkably well reproduced in both amplitude and penetrating depth as in the observations. Although the PV anomalies are mostly confined to the stratosphere, our results confirm that its downward influences are sufficiently strong such that associated tropospheric anomalies with the stratospheric PV are capable of triggering the cold surge occurrence within the given mechanism.

Key words: Cold surge, downward control, piecewise potential vorticity inversion, Siberian High, stratospheric potential vorticity

1. Introduction

Since Charney and Drazin (1961), the linear wave dynamics of vertical propagation of Rossby waves has been a solid paradigm in the coupling of the stratosphere and troposphere. Deceleration of the polar night jet by the interaction between zonal mean and eddy potential vorticies that propagated from the troposphere as quasi-stationary planetary waves often leads to sudden stratospheric warming events (Holton, 2004). However, relatively little is known about the reverse process; the stratospheric influence on the troposphere. Some observational analyses support the idea that the stratospheric potential vorticity (PV) anomaly influences tropospheric circulations (Hartley *et al.*, 1998; Baldwin and Dunkerton, 1999; Christiansen, 2001; Ambaum and Hoskins, 2002; Thompson *et al.*, 2002; Nakagawa and Yamazaki, 2005). The modeling study of Marshall *et al.* (2009) further supports the premise that the inclusion of stratospheric information substantially improves seasonal winter forecasts.

Although the precise mechanism of the downward propagation from the stratosphere is still not clear, it has recently become more acceptable that the downward propagation is mainly due to the geostrophic and hydrostatic adjustment processes from the existing stratospheric PV anomaly (Hoskins *et al.*, 1985; Ambaum and Hoskins, 2002; Black *et al.*, 2002).

As one of the most conspicuous weather events in East Asia during winter, cold surges (CS) largely influence many human activities. With an expansion of the Siberian High, extremely cold air that piles up north of the Tibetan plateau is abruptly brought to East Asia in a few days. A typical East Asian CS is accompanied by the upper tropospheric short-wave trough over Lake Baikal that grows by propagating toward East Asia (Joung and Hitchman, 1982; Chen *et al.*, 2004; Park *et al.*, 2008).

From a detailed lagged composite analysis of CS

Corresponding Author: Dr. Seong-Joong Kim, Korea Polar Research Institute, PO Box 32, Inchon 406-840, Republic of Korea.
Phone : +82-32-260-6232, Fax : +82-32-260-6109
E-mail: seongjkim@kopri.re.kr

events over the past 40 years using NCEP/NCAR reanalysis (Kalnay *et al.*, 1996), Jeong *et al.* (2006) detected a precursory signal in the stratosphere prior to CS occurrence in East Asia. About one week before the CS occurrence, strong stratospheric negative PV anomalies and rising geopotential height in the troposphere were observed over northern Asia. The influence of the stratospheric PV has been generally regarded as incapable of driving the tropospheric anomaly because of the relatively small fraction of mass of air in the stratosphere compared to the troposphere. However, the lagged composite analyses indicated that the stratosphere influences the troposphere with deep penetrating circulation anomalies.

To establish a dynamical reason for the features found in the statistical analysis by Jeong *et al.* (2006), in the present study, we investigate the role of stratospheric PV to determine whether it amplifies the Siberian High through geostrophic and hydrostatic adjustment processes propagating from the PV source and eventually penetrates into the tropopause. We have adopted the piecewise PV inversion technique developed by Davis (1992). The dynamically balanced circulation is compared with the lagged composite circulations obtained by CS index.

Section 2 is devoted to the description on the lagged composite features of the precursory stratospheric PV signal and tropospheric evolution of relevant circulations before the CS. In section 3, the procedure of piecewise PV inversion is described. Section 4 shows the result of piecewise PV inversion and compares the balanced circulation obtained by prescribed PV source with the lagged composite circulation.

2. Stratospheric PV as a precursor for cold surge

Jeong *et al.* (2006) found that about one week ahead of CS occurrence the large-scale positive anomaly of geopotential height emerges in the upper troposphere over central Siberia accompanied with strong negative PV anomalies aloft in the lower stratosphere. In present study we repeat their composite analyses and re-examine some important large-scale precursory signals before CS occurrence. From about lag of -10 days of the CS occurrence, strong positive anomalies of geopotential height exist in the upper troposphere over Siberia forming a zonally elongated large-scale structure (Fig. 1b). At the same time, a large stationary negative PV anomaly is also captured in the stratosphere (Fig. 1a). This negative anomaly is quite stationary and does not change much from -10 days to -5 days, after which it slowly moves southeastward as the CS event approaches (Figure not shown). The peak PV value reaches about 7 PVU, where 1 PVU (PV unit) is defined as 10^{-6} m^2 s^{-1} K kg^{-1}. Compared to the climatological PV at 20 hPa during the winter, 7 PVU is quite big.

On the CS occurrence day (lag=0), this upper-level anomaly appears to transform into the propagating wave pattern of the northwest-southeast orientation (Fig. 1c). Based on the criteria of CS occurrence (Jeong *et al.*, 2005), the downstream development of this upper-level wave advects cold air of at least 4 K lower than normal into Korean peninsula, Japan and China. In the lower stratosphere, the large stationary negative PV vortex is found over the positive geopotential height in upper troposphere. More detailed dynamical features associated with the upper-level precursory signal can be seen in the pressure-longitude sections of Fig. 2, which show the composite vertical structures of PV, potential temperature, and geopotential height anomalies along 60°N averaged from 10 to 7 days before the cold surge occurrence day. The composites reveal that below the negative PV anomaly the strong positive potential temperature anomaly extends from the lower stratosphere to the upper troposphere, while slightly above the negative PV source there exist negative potential temperature anomalies, showing the overall dipolar structure. In the regions below the negative PV anomalies, the positive geopotential height anomalies further extend down towards the upper troposphere reaching at 300 hPa (Fig. 2c). The coexisting positive potential temperature and geopotential height anomalies appear to satisfy the thermal wind balance. Therefore these vertical structures seem to be well constrained by the PV anomaly.

As suggested in Jeong *et al.* (2006), the upper-tropospheric perturbation over Siberia may trigger the initial growth of the CS. The composite results described above indicate that the upper-tropospheric

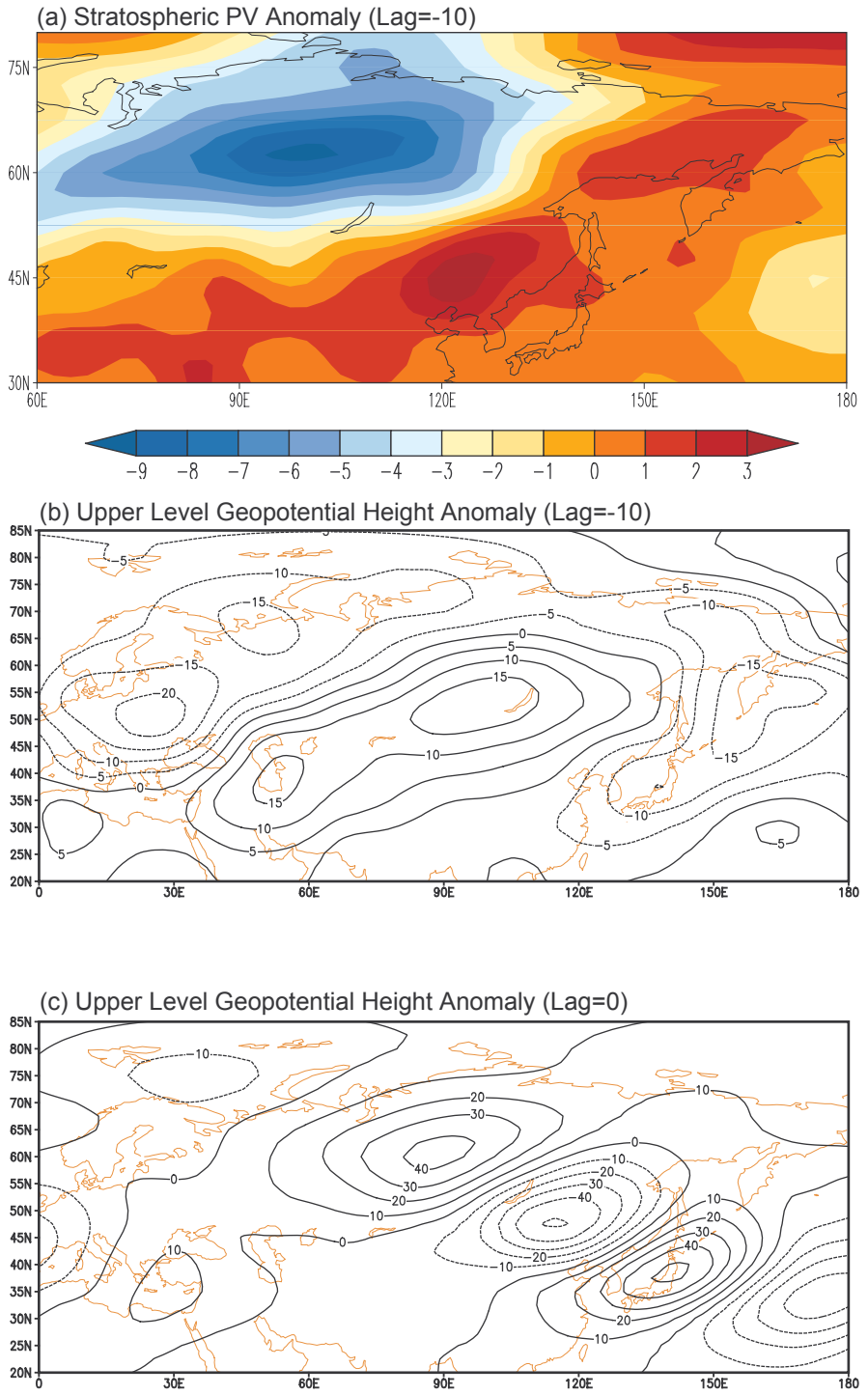

Fig. 1. Lagged composite analysis of (a) PV anomaly at 20 hPa with -10 days lag, (b) geopotential height anomaly at 300 hPa with -10 days lag, and (c) geopotential height anomaly at 300 hPa with 0 day lag.

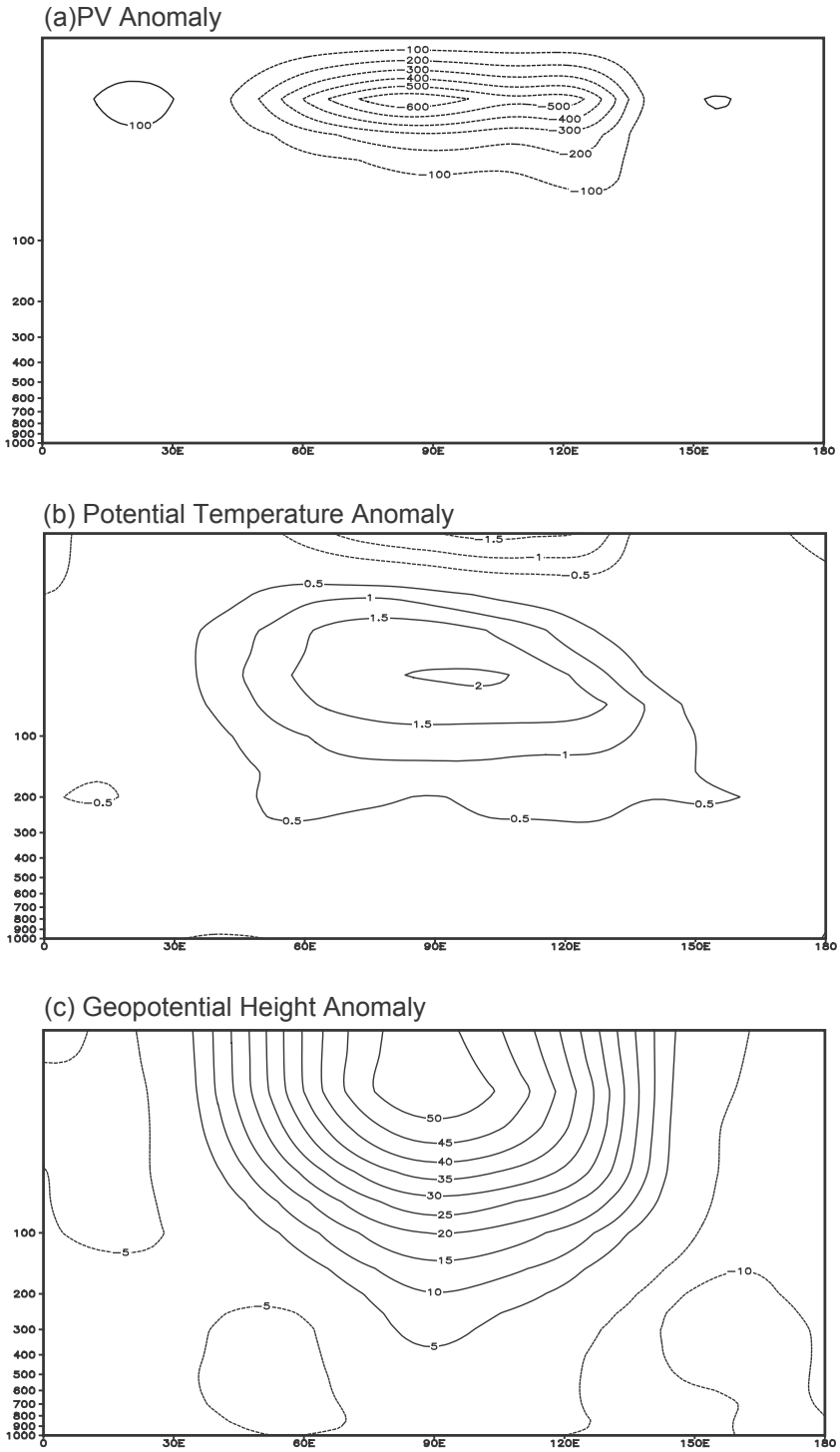

Fig. 2. Pressure-longitude cross-section of lagged composite at 60°N for (a) PV anomaly (Contour; 0.01PVU), (b) potential temperature anomaly (Contour; 0.5 K), and (c) geopotential height anomaly (Contour; m) averaged over 10 to 7 days before the cold surge.

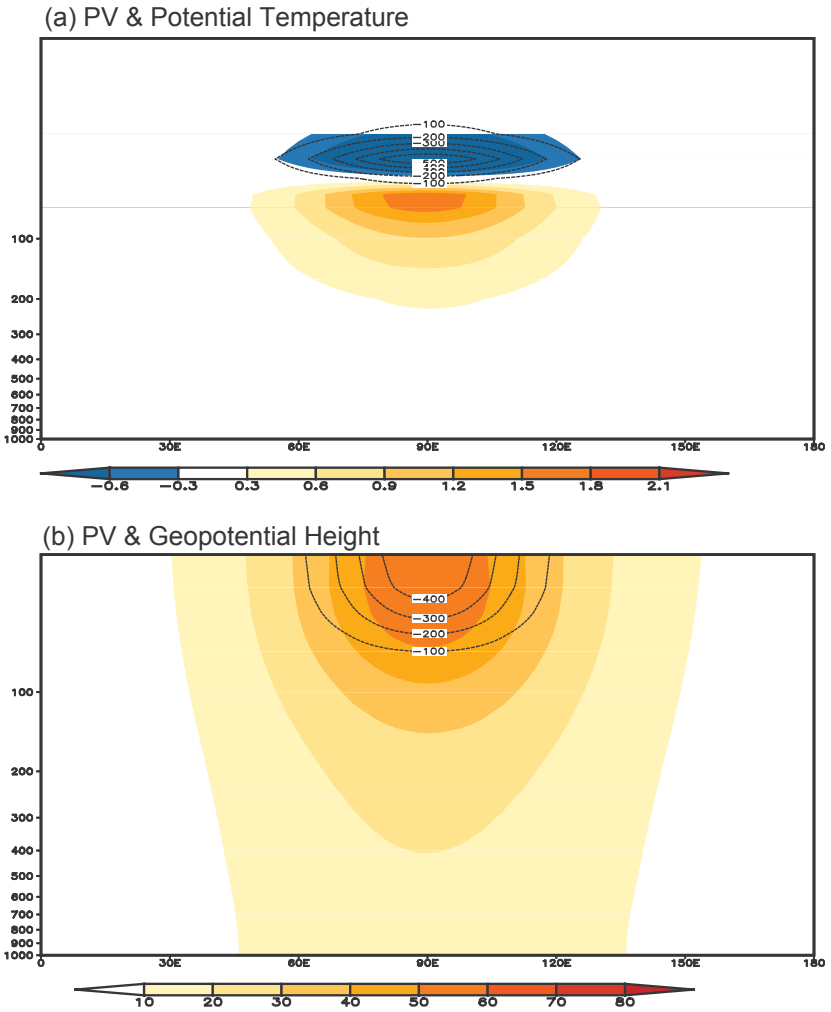

Fig. 3. The balanced (a) potential temperature (K) and (b) geopotential height (m) anomaly (shaded) of prescribed PV anomaly (contours). Contour interval is 0.01 PVU.

perturbation seems to be directly induced from the stratospheric PV anomaly. In the following sections we will quantify to what extent the stratospheric PV anomalies induce the upper-tropospheric perturbation by applying the piecewise PV inversion technique. The PV and potential temperature composite results here will be used for this.

3. Formulation of PV inversion

Ertel potential vorticity (EPV), in its original form, is defined as the dot product of the absolute vorticity and the three dimensional potential temperature gradient divided by air density,

$$EPV = \frac{1}{\rho}\vec{\eta}\cdot\nabla\theta \quad . \tag{1}$$

EPV is a conserved quantity that contributes to an early foundation of geophysical fluid dynamics, especially quasi-geostrophic dynamics in explaining the midlatitude baroclinic eddies (Hoskins *et al.*, 1985).

In addition to the importance by its conservation

property, EPV can be used to analyze large-scale motion constrained by geostrophic and hydrostatic balance. In the so called 'PV thinking' paradigm, the 3-dimensional distribution of EPV immediately yields the temperature and wind fields which are consistent (balanced) with the EPV. This nice property is related to the fact that EPV is just a multiple of absolute vorticity and static stability which essentially corresponds to the spatial structures of wind and temperature fields. The integrated nature of EPV makes it possible to separate wind and temperature parts from the given EPV if proper conditions are provided. The conditions for the separation are 1) large scale constraints such as geostrophic and hydrostatic balance and 2) proper boundary conditions guaranteeing the unique separation. This separation is usually called PV inversion.

In the literature there are two representations of EPV according to the choice of vertical coordinates. For the identification of disturbances in the map and the theoretical studies which benefits the conservation of adiabatic motion along the isentropic surface, the isentropic coordinate is preferred and it is referred to as isentropic potential vorticity (IPV). IPV is written as

$$IPV = -g\left(f + \vec{k}\cdot\nabla_\theta \times \vec{V}\right)\frac{\partial p}{\partial \theta}. \tag{2}$$

where g is the gravitational force, f is the Coriolis parameter, θ is potential temperature, $\vec{V}$ is the 3-dimensional wind, and p is pressure. However for computational purposes, the isobaric coordinate version of PV is preferred for two reasons. First, most datasets including state of the art reanalyses adopts isobaric coordinates for the representation. Henceforth, formulating PV inversion in isobaric coordinates helps to reduce errors caused by coordinate interpolation. Second, isobaric formulation with the introduction of the exner-function Π, which shares the same coordinate line with basic pressure coordinates helps to express boundary conditions for PV inversion. The exner-function is defined as

$$\Pi = C_p\left(\frac{p}{p_0}\right)^{\kappa}. \tag{3}$$

The upper and lower boundary conditions for PV Inversion are taken by specifying potential temperature distribution at those surfaces (Bretherton, 1966). According to Bretherton (1966), surface potential temperature can be regarded as potential vorticity. In Π-coordinate, hydrostatic balance is expressed as

$$\frac{\partial \Phi}{\partial \Pi} = -\theta. \tag{4}$$

This expression is not only simple but also provides the easiest way to incorporate the boundary condition. In isobaric coordinates, EPV is expressed as

$$\begin{aligned} PV &= -g(f\vec{k} + \nabla_p \times \vec{V})\cdot\nabla_p\theta \\ &\cong -g\left[\frac{\partial u}{\partial p}\frac{\partial \theta}{\partial y} - \frac{\partial v}{\partial p}\frac{\partial \theta}{\partial x} + (\zeta + f)\frac{\partial \theta}{\partial p}\right] \\ &= -\frac{g\kappa\Pi}{p}\left[\eta\frac{\partial \theta}{\partial \Pi} - \frac{\partial v}{\partial \Pi}\frac{\partial \theta}{\partial x} + \frac{\partial u}{\partial \Pi}\frac{\partial \theta}{\partial y}\right]. \end{aligned} \tag{5}$$

The last expression is derived by using the coordinate transform unit from pressure to the exner-function.

$$\frac{\partial \Pi}{\partial p} = C_p\kappa\left(\frac{p}{p_0}\right)^{\kappa-1}\frac{1}{p_0} = \frac{\kappa\Pi}{p}. \tag{6}$$

Using rotational wind instead of the full wind field and using the hydrostatic equation in spherical horizontal coordinates, PV is expressed as

$$\begin{aligned} PV = \frac{g\kappa\Pi}{p}\Bigg[&\left(f + \nabla^2\Psi\right)\frac{\partial^2\Phi}{\partial\Pi^2} \\ &- \frac{1}{a^2\cos^2\phi}\frac{\partial^2\Psi}{\partial\lambda\partial\Pi}\frac{\partial^2\Phi}{\partial\lambda\partial\Pi} - \frac{1}{a^2}\frac{\partial^2\Psi}{\partial\phi\partial\Pi}\frac{\partial^2\Phi}{\partial\phi\partial\Pi}\Bigg]. \end{aligned} \tag{7}$$

Thus, PV is completely determined by the 3-dimensional distribution of both Ψ (streamfunction) and Φ (geopotential). In large scale motion, Ψ and Φ are highly related because of the earth's rotation and subsequent horizontal stratification. For this, the geostrophic relation is usually adopted (Hartley *et al.*, 1998; Black, 2002). However, Davis (1992) uses

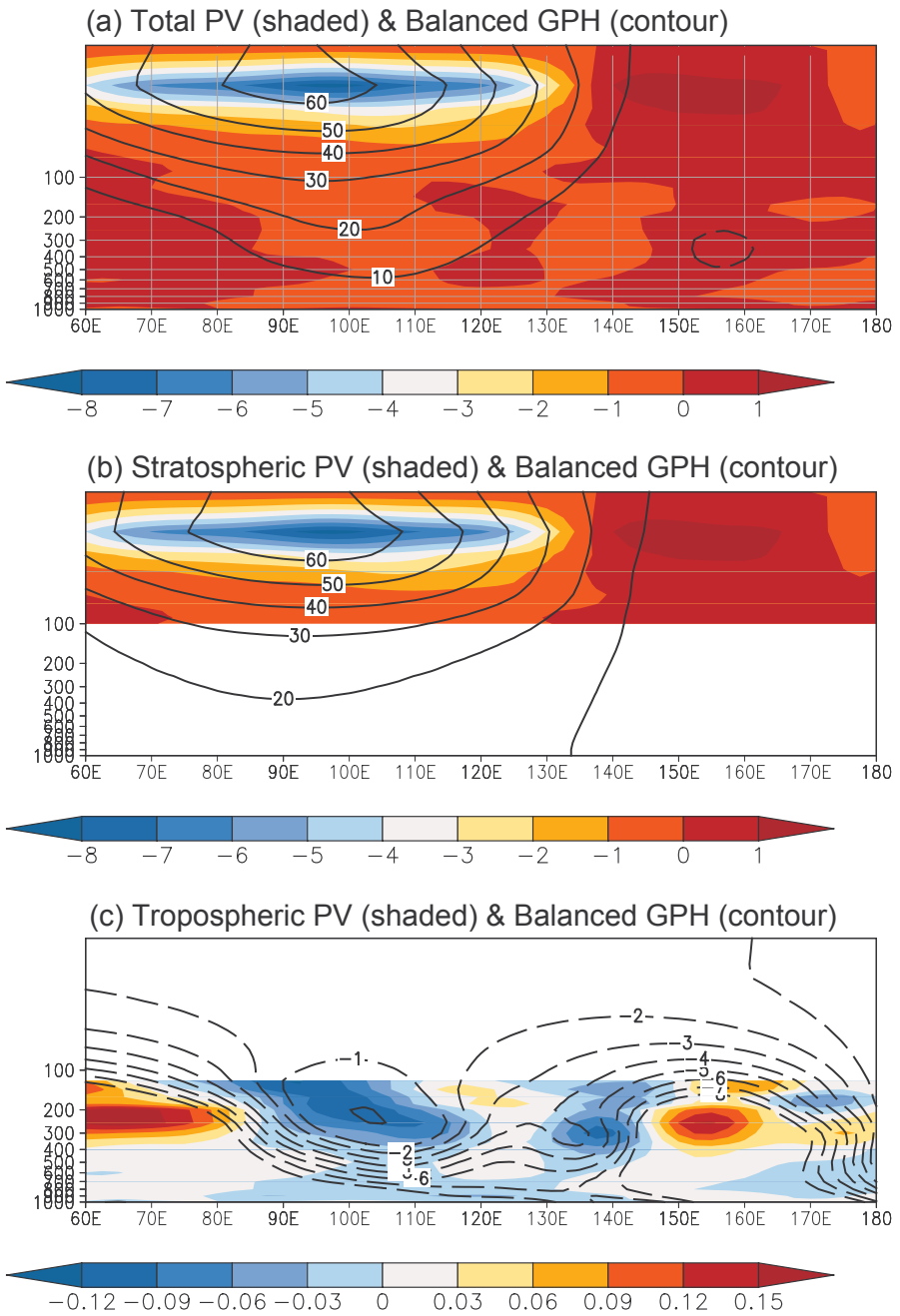

Fig. 4. Longitude-pressure cross-section of balanced geopotential height (contour) at 60°N according to lagged composite (shaded) of (a) total PV, (b) stratospheric PV (above 100 hPa), and (c) tropospheric PV (below 100 hPa). Lag -10 PV is depicted. Units are m for geopotential height and PVU for PV.

gradient wind balance to extend the applicability of PV inversion to mesoscale dynamics. The balance implied is similar to geostrophic but an additional term is included in order to account for the acceleration

due to the curvature of the pressure system. The condition reads

$$\nabla^2\Phi = \nabla\bullet\left(f\nabla\Psi\right) + \frac{2}{a^4\cos^2\phi}\frac{\partial\left(\partial\Psi/\partial\lambda,\partial\Psi/\partial\phi\right)}{\partial\left(\lambda,\phi\right)}. \quad (8)$$

Now, the PV inversion problem is simply defined by Eqs. (4), (7) and (8). Given specified PV on the left-hand side of Eq. (7), we can solve the inversion to yield Ψ and Φ using Eqs. (7) and (8) with the specified boundary condition (4).

Additionally, Davis (1992) derived a formula for piecewise PV inversion. The piecewise PV inversion allows us to separate the impact of each PV piece. For instance, the impact of stratospheric or tropospheric PV on Ψ and Φ can be estimated separately by this technique. In the original form, the formula contains a small contribution from nonlinear terms, but, in this study, we simply linearize it to drop the small contribution from the nonlinear terms. After linearization, Eqs. (7) and (8) become

$$\begin{aligned} q' = &\left(f+\nabla^2\bar{\Psi}\right)\frac{\partial^2\Phi'}{\partial\Pi^2}+\frac{\partial^2\bar{\Phi}}{\partial\Pi^2}\nabla^2\Psi' \\ &-\frac{\partial^2\bar{\Phi}}{\partial x\partial\Pi}\frac{\partial^2\Psi'}{\partial x\partial\Pi}-\frac{\partial^2\bar{\Psi}}{\partial x\partial\Pi}\frac{\partial^2\Phi'}{\partial x\partial\Pi} \\ &-\frac{\partial^2\bar{\Phi}}{\partial y\partial\Pi}\frac{\partial^2\Psi'}{\partial y\partial\Pi}-\frac{\partial^2\bar{\Psi}}{\partial y\partial\Pi}\frac{\partial^2\Phi'}{\partial y\partial\Pi}, \end{aligned} \quad (9)$$

$$\begin{aligned} \nabla^2\Phi' = &\nabla\cdot\left(f\nabla\Psi'\right) \\ &+2\left(\frac{\partial^2\bar{\Psi}}{\partial x^2}\frac{\partial^2\Psi'}{\partial y^2}+\frac{\partial^2\bar{\Psi}}{\partial y^2}\frac{\partial^2\Psi'}{\partial x^2}\right. \\ &\left.-2\frac{\partial^2\bar{\Psi}}{\partial x\partial y}\frac{\partial^2\Psi'}{\partial x\partial y}\right), \end{aligned} \quad (10)$$

subject to the perturbation boundary condition $\frac{\partial\Phi'}{\partial\Pi}=0$ at the top and bottom. All the following results in this study are obtained by solving Eqs. (9) and (10) simultaneously.

4. Results

a. Response to idealized PV source

We first test the PV inversion with the idealized PV anomaly which mimics the 3-dimensional PV features in Fig. 2a. A Gaussian type disturbance is used for the idealized PV anomaly,

$$PV' = 300\exp\left[-\frac{\left(x-90^\circ\mathrm{E}\right)^2}{\sigma_x^{\,2}}-\frac{\left(y-60^\circ\mathrm{N}\right)^2}{\sigma_y^{\,2}} -\frac{\left(p-40\ \mathrm{hPa}\right)^2}{\sigma_p^{\,2}}\right], \quad (11)$$

where, $\sigma_x^{\,2}=3000$, $\sigma_y^{\,2}=3000$, and $\sigma_p^{\,2}=400$. This idealized PV anomaly resides only in the lower stratosphere. The basic state ($\bar{\Psi}$, $\bar{\Phi}$) in Eqs. (9) and (10) are obtained by another PV inversion using Eqs. (7) and (8) with the prescribed PV calculated by the 1958-2001 winter climatological wind and temperature.

Figure 3 shows the balanced potential temperature and geopotential height obtained by piecewise PV inversion with the specified PV anomaly given in Eq. (11). In Fig. 3a, the positive potential temperature anomaly penetrates into the upper tropopause and exhibits the dipolar structure with a maximum of about 2 K at 100 hPa. Compared to the warm anomaly, the cold anomaly is rather weak and is placed slightly above the PV source level. This balanced thermal structure which appears around the isolated PV anomaly is consistent with results suggested in previous studies (Hoskins *et al.,* 1985; Ambaum and Hoskins, 2002). The warming below the PV source can be interpreted as the bending isentropic surface toward (away from) the localized positive (negative) PV source. Because one of the purposes for conducting the piecewise PV inversion is to examine in detail whether the PV derived anomalies can penetrate the tropopause, this is one of key mechanisms explaining the downward propagation of the stratospheric PV signal. From Figs. 3a and 3b, it is clearly seen that

the balanced anomaly penetrates the tropopause. Hoskins *et al.* (1985) suggested that the penetration depth is proportional to fL/N. Here, L is horizontal scale of the PV disturbance and N is buoyancy frequency. According to this, it is expected that the large horizontal scale of the prescribed PV disturbance covering almost the entire northern Eurasian continent is sufficient to contribute to the deep penetration of the induced flow.

Comparing the balanced potential temperature anomaly of Figs. 2b and 3a, it is seen that they are very similar both in magnitude and in vertical dipolar structure. Considering the crude nature of the implemented PV anomaly, this is quite an inspiring result. The vertical structure of the balanced geopotential height is a funnel-like shape extending from the stratosphere to the troposphere (Fig. 3b). At the surface, the balanced geopotential height is more than 10m which is not small compared to the magnitude of typical weather disturbances such as baroclinic eddies. The structures depicted in Figs. 2c and 3b are also very similar especially in the stratosphere and upper troposphere.

This result strongly suggests that the features of the lagged composite analysis shown in Fig. 2 are not artifacts of statistical analysis but are due to the dynamical adjustment of geostrophic and hydrostatic balance propagated from the stratospheric PV anomaly. Henceforth, this gives more confidence that the precursory signal found in the stratosphere ahead of the CS provides the initial perturbation in the upper troposphere. As seen in the composite geopotential height field on the CS occurrence day (Fig. 1b), this initial perturbation grows into a northwest–southeast elongated baroclinic eddy which transports cold air piled up over Siberia downstream, eventually manifesting the CS event.

b. Response to observed stratospheric PV source

Finally, we applied the PV inversion to the composite of the observed PV anomaly which is believed to be the precursory signal of CS occurrence. The PV inversion is applied to the composite PV anomaly on day -10. The balanced circulations from PV for the entire level (Fig. 4a), for the stratosphere (above 100 hPa; Fig. 4b), and for the troposphere (below 100 hPa; Fig. 4c) are estimated separately by the piecewise PV inversion technique. Results clearly demonstrate that the balanced geopotential in the troposphere mostly originates from the stratosphere and is weakly modified by the tropospheric origin. Comparing Fig. 4b and 4c, it is evident that the balanced geopotential anomaly derived by tropospheric PV anomaly is much weaker than that of the stratospheric anomaly (note the different contouring used in the panels of Fig. 4). Notably, the tropospheric PV source makes the vertical axis of the ridge tilt towards the west. This indicates that the tropospheric PV structure corresponds to the developing baroclinic eddy.

5. Summary and discussion

The idea for this paper arose from the finding of Jeong *et al.* (2006): Strong coupling between the stratosphere and troposphere is responsible for the initiation of CS occurrence in East Asia. Strong negative PV in the stratosphere was suggested as the precursory circulation which directly induces the upper tropospheric perturbation. In the present study we have tested this conjecture dynamically by using the piecewise PV inversion technique.

In conclusion, the inversion results strongly suggest that the stratospheric PV is capable of driving tropospheric circulation anomalies with a sufficient magnitude to initiate a CS event. However, this does not imply that the mechanism described here is solely responsible for CS occurrence. Also the linkage found by piecewise PV inversion is purely diagnostic and does not support any specific propagating mechanism. Some previous studies indicate that, from a few days before the CS, an upper level disturbance over Western Europe propagates downstream and develops into a CS event (Joung and Hitchman, 1982; Sung *et al.*, 2009). Considering these studies explaining different origins of CS event, the assessment of the predictability of stratospheric PV in the forecast of CS event is important. The predictability can be practically estimated by success and false alarm rates of CS occurrence for the given stratospheric PV.

There remains one unresolved interesting question: How does such a large negative PV anomaly come out, in particular, over the Siberia about a week before the CS? To examine this, the wave propagation from the various sources in the troposphere should be examined. Along with this, a few studies examined snow cover perturbation as a source for the stratospheric PV anomaly (Lu *et al.,* 2008; Fletcher *et al.*, 2009*)*. The vertical propagation of wave activity triggered by the snow cover anomaly can drive the wave-mean flow interaction in the stratosphere which, in turn, propagates downward.

Acknowledgements. Yoo-Jin Kim of Korea Polar Research Institute is appreciated for her help in preparation and analysis of potential vorticity. The contribution of the second author, Jee-Hoon Jeong, is the contribution No. 29 from TELLUS, the centre of Earth System Science at University of Gothenburg. Useful comments and their efforts by two anonymous reviewers greatly helped improve manuscript. This study was supported by the projects of Studies on the Polar Atmosphere and Climate Change (PE09030) and Paleoclimate Modeling Study for Polar Regions (PE09120) of the Korea Polar Research Institute.

REFERENCES

Ambaum, M. H. P., and B. J. Hoskins, 2002: The NAO troposphere-stratosphere connection. *J. Climate*, **15**, 1969-1978.

Baldwin, M. P., and T. J. Dunkerton, 1999: Propagation of the Arctic Oscillation from the stratosphere to the troposphere. *J. Geophys. Res.*, **104**, 30937-30946.

Black, R. X., 2002: Stratospheric forcing of surface climate in the Arctic Oscillation. *J. Climate*, **15**, 268-277.

Bretherton, F. P., 1966: Critical layer instability in baroclinic flows. *Quart. J. Roy. Meteor. Soc.*, **92**, 325-334.

Charney, J. G., and P. G. Drazin, 1961: Propagation of planetary-scale disrurbances from the lower into the upper atmosphere. *J. Geophys. Res.*, **66**, 83-109.

Chen, T.-C., W.-R. Huang, and J.-H. Yoon, 2004: Interannual variation of the East Asian cold surge activity. *J. Climate*, **34**, 293–305.

Christiansen, B., 2001: Downward propagation of zonal mean zonal wind anomalies from the stratosphere to the troposphere: model and reanalysis. *J. Geophys. Res.*, **106**, 27307-27322.

Davis, C. A., 1992: Piecewise potential vorticity inversion. *J. Atmos. Sci.*, **49**, 1397-1411.

Fletcher, C. G., S. C. Hardiman, P. J. Kushner, and J. Cohen, 2009: The dynamical response to snow cover perturbations in a large ensemble of atmospheric GCM integrations. *J. Climate*, **22**, 1208-1222.

Hartley, D. E., J. T. Villarin, R. X. Black, and C. A. Davis, 1998: A new perspective on the dynamical link between the stratosphere and troposphere. *Nature*, **391**, 471-474.

Holton, J. R., 2004: *An Introduction to Dynamic Meteorology.* Elsevier, 529 pp.

Hoskins, B. J., M. E. McIntyre, and A. W. Robertson, 1985: On the use and significance of isentropic potential vorticity maps. *Quart. J. Roy. Meteor. Soc.*, **111**, 877–946.

Jeong, J. H., B. M. Kim, C. H. Ho, D. Chen, and G. H. Lim, 2006: Stratospheric origin of cold surge occurrence in East Asia. *Geophys. Res. Lett.*, **33**, L14710, doi:10.1029/2006GL026607.

_____, and C.-H. Ho, 2005: Changes in occurrence of cold surges over East Asia in association with Arctic Oscillation. *Geophys. Res. Lett.*, **32**, L14704, doi:10.1029/2005GL023024.

Joung, C. H., and M. H. Hitchman, 1982: On the role of successive downstream development in east Asian polar air outbreaks. *Mon. Wea. Rev.*, **110**, 1224-1237.

Kalnay, E., and Coauthors, 1996: The NCEP/NCAR 40-year reanalysis project. *Bull. Amer. Meteor. Soc.*, **77**, 437–471.

Lu, J. M., J. H. Ju, S. J. Kim, J. Z. Ren, and Y. X. Zhu, 2008: Arctic Oscillation and the autumn/winter snow depth over the Tibetan Plateau. *Geophys. Res. Lett.*, **113**, D14117, doi:10.1029/2007JD009567.

Marshall, A. G., A. A. Scaife, and S. Ineson, 2009: Enhanced seasonal prediction of European winter warming following volcanic eruptions. *J. Climate*, early online release, doi:10.1175/2009JCLI3145.1.

Nakagawa, K. I., and K. Yamazaki, 2005: What kind of stratospheric sudden warming propagates to the troposphere? *Geophys. Res. Lett.*, **33**, L04801, doi:10.1029/2005GL024784.

Park, T.-W., J.-H. Jeong, C.-H. Ho, and S.-J. Kim, 2008: Characteristics of atmospheric circulation associated with cold surge occurrences in east Asia: A case study during 2005/06 winter. *Adv. Atmos. Sci.*, **25**, 791-804.

Sung, M.-K., G.-H. Lim, W.-T. Kwon, K.-O. Boo, and J.-S. Kug, 2009: Short-term variation of Eurasian pattern and its relation to winter weather over East Asia. *Int. J. Climatol.*, **29**, 771-775.

Thompson, D. W. J., M. P. Baldwin, and J. M. Wallace, 2002: Stratospheric connection to Northern Hemisphere wintertime weather: implications for prediction. *J. Climate*, **15**, 1421-1428.

Zhang, Y., K. R. Sperber, and J. S. Boyle, 1997: Climatology and interannual variation of East Asian winter monsoon: result from the 1979-95 NCEP/NCAR reanalysis. *Mon. Wea. Rev.*, **125**, 2605-2619.